**Author Manuscript:**
Published in final edited form as: *e-Journal of Surface Science and Nanotechnology* ***21****, 114−120 (2023)*
DOI: 10.1380/ejssnt.2023-038

# Electron Inelastic Scattering in Surface Analysis

Shigeo Tanuma †

*Materials Data Platform Center, National Institute for Materials Science, 1-1 Namiki, Tsukuba, Ibaraki 305-0044, Japan* †
*Corresponding author: tanuma-sh@tbd.t-com.ne.jp, tanuma.shigeo@nims.go.jp*

**Electron inelastic scattering in Surface Analysis**

Shigeo Tanuma*

Materials Data Platform Center, National Institute for Materials Science, 1-1 Namiki, Tsukuba, Ibaraki 305-0044

（Received XXX XX, 20XX ; Accepted XXX XX, 20XX

This paper discusses the recent progress in electron inelastic mean free paths (IMFPs) calculations with the dielectric response function and optical energy loss function (ELF) as key parameters. For most materials, the IMFP values calculated using various algorithms show good agreements with each other in the energy region above 300 eV; however, a large difference exists in the energy region under 200 eV. The energy dependencies of IMFPs calculated from optical ELFs can be expressed using the modified Bethe equation for energy regions between 50 eV and 200 keV; the material dependence of IMFPs can be expressed by the TPP-2M equation. For IMFP calculations, the treatments and evaluations of the electron exchange effect, the effect of energy gap in the energy loss function, and the associated integral region remain important issues that will need to be addressed in the future.

KEYWORDS: electron inelastic mean free path, dielectric function model, energy loss function, modified Bethe equation

## 1. Introduction

Information on electron inelastic scattering in solids is required in various fields, from surface analysis with Auger electron spectroscopy (AES) and X-ray photoelectron spectroscopy (XPS), to thin film analysis using X-ray absorption fine structure (XAFS), radiation physics, radiation transport, and transmission electron microscope (TEM). The most important and fundamental parameter for applications is the electron inelastic mean free path (IMFP). In surface analysis, IMFP is a good indicator of surface sensitivity.

IMFP, $\lambda$, is simply related to the total cross section for inelastic scattering $\sigma$ and the number of atoms per unit volume in the solid $N$,

$$\lambda = \frac{1}{\sigma N}, \qquad (1)$$

In JIS K-0147(2017)[1], IMFP is defined as "average distance that an electron with a given energy travels between successive inelastic collisions". In actual theoretical calculations, IMFP is determined from the inelastic scattering cross section using Equation (1).

In surface analysis, IMFP is not only a physical quantity that expresses surface sensitivity when analyzed by AES or XPS, but is also closely related to electron effective attenuation length (EAL) and mean escape depth (MED), which are frequently used in actual applications such as film thickness measurement. Usually, these parameters are derived from the IMFP values (See Reference 10). Therefore, there have been many studies on the calculations and measurements of IMFP.

In this paper, I will summarize the progress of IMFP calculations based on the dielectric function model, focusing on progress since 2000. I would also like to clarify the

current status and issues. The results of research on IMFP up to 1999 have been summarized appropriately in the review by Powell-Jablonski [2].

## 2. IMFP calculations

### 2.1 Overview of IMFP calculations using the dielectric function model

IMFP is now commonly calculated from the energy loss function (ELF) of the material, the so-called dielectric function model. In the energy regions of ≤500 keV, the differential cross section $\sigma_{in}$ in inelastic scattering is given by the relativistic quantum theory, and under the Born approximation, the differential cross sections (DCS) for scattering per atom is given as[3,4,5]

$$\frac{\mathrm{d}^2\sigma_{in}}{\mathrm{d}W\mathrm{d}Q} \approx \frac{2\pi e^4}{m_e v^2}\frac{1+Q/m_e c^2}{Q(1+Q/2m_e c^2)}\frac{2}{\pi\Omega_p^2}\mathrm{Im}\left(\frac{-1}{\epsilon(Q,W)}\right), \quad (2)$$

where $W$, $Q$, $m_e, v, c$,Im$(-1/\epsilon)$, and $\Omega_p$ represent the energy loss, recoil energy, electron mass, electron velocity, light velocity, energy loss function, and plasmon energy, respectively.

When this equation uses atomic units ($m_e = e^2 = \hbar = 1$), $Q$ is replaced with momentum transfer $q$, and $W$ is replaced with $\omega$ ($= \hbar\omega$), it becomes[6]

$$\frac{d^2\sigma_{in}}{d\omega dq} \approx \frac{2}{\pi N v^2}\mathrm{Im}\left[\frac{-1}{\varepsilon(q,\omega)}\right]\frac{1}{q}, \quad (3)$$

Therefore, if $\mathrm{Im}[-1/\varepsilon(q,\omega)]$ for target material is known, IMFP can be computed through Equation (1). That is,

$$\lambda(T)^{-1} = \frac{1}{\pi T\cdot F(T)}\iint_D \mathrm{Im}\left[\frac{-1}{\varepsilon(\omega,q)}\right]\frac{1}{q}dqd\omega, \quad (4)$$

where $F(T)$ represents the correction coefficient of the relativistic effect. Integral domain $D$ is determined from the maximum and minimum energy loss, and the maximum and minimum kinematically permissible momentum transfer.

### 2.2 IMFP calculation algorithm

A major issue in IMFP calculations using a dielectric function is determining the energy loss function $\mathrm{Im}[-1/\varepsilon(q,\omega)]$. Research has focused on this challenge for the past 20 years. That is, $\mathrm{Im}[-1/\varepsilon(q,\omega)]$ is unknown for most materials. The optical constants have been measured across a sufficiently wide range of energy regions in only a very small number of materials, from which the optical ELF $\mathrm{Im}[-1/\varepsilon(\omega)]$ can be determined. Therefore, to determine the $q$-dependence of $\mathrm{Im}[-1/\varepsilon(q>0,\omega)]$, an algorithm is needed to extend the dielectric function to the $q > 0$ region.

1) Penn algorithms

Penn determined the $\mathrm{Im}[-1/\varepsilon(q,\omega)]$ of the target material in Equation (3) from the optical ELF $\mathrm{Im}[-1/\varepsilon(\omega)]$ and the Lindhard model dielectric function and proposed an algorithm to calculate IMFP. [7] This method is now known as the full Penn algorithm (FPA). In the FPA, the ELF in Equation (3) is given as

$$\mathrm{Im}\left[\frac{-1}{\varepsilon(q,\omega)}\right] = \int_0^\infty d\omega_p g(\omega_p)\mathrm{Im}\left[\frac{-1}{\varepsilon_L(q,\omega;\omega_p)}\right], \quad (5)$$

where $\varepsilon_L$ represents the Lindhard dielectric function for free electron gas [8,9]. Further, $\omega_p$, $n$, and $g(\omega_p)$ represent the plasmon energy ($= \sqrt{4\pi n}$), electron density, and coefficient satisfying $\mathrm{Im}[-1/\varepsilon(q=0,\omega)] = \mathrm{Im}[-1/\varepsilon(\omega)]$, respectively. $g(\omega_p)$is given as

$$g(\omega) = \frac{2}{\pi\omega}\mathrm{Im}\left[\frac{-1}{\varepsilon(\omega)}\right]. \quad (6)$$

Detailed information on the specific calculation is presented in references 6 and 10.

There is also a simplified version of Penn algorithm (SPA) that introduces a single-pole approximation, and in the energy region above 200 eV, the IMFPs calculated with SPA agree well with the FPA results [7].

Tanuma–Powell–Penn used experimentally determined optical ELF for 27 types of elemental solids [11,12], 15 types of inorganic compounds [13], and 14 types of organic compounds [14], and they calculated the electron IMFPs from 50 eV to 2,000 eV with a nonrelativistic Penn algorithm [7].

Shinotsuka *et al.* used relativistic FPA to extend IMFP to an electron energy of 200 keV for 41 elemental solids [15], 42 inorganic compounds [16], 14 organic compounds, and water [17], and prepared an IMFP database from 50 eV to 200 keV to provide IMFP data on high-energy regions that are required for hard X-ray photoelectron spectroscopy (HAXPES) and TEM.

The number of ELF data is insufficient for inorganic

compounds, and therefore, Shinotsuka *et al*. calculated the optical constants for more than 30 compound semiconductors and non-conductors using WIEN2k[18] and FEFF codes [19]. Further, they prepared a highly accurate optical ELF database covering a broad energy range (0.1 eV–1 MeV) [20]. Their calculations significantly improved the accuracy of IMFPs compared to the earlier work of Tanuma *et al.* [21]. They also introduced an algorithm proposed by Boutboul *et al.* [22] to consider the band gap $E_g$ for non-conductors. Then the IMFPs can be calculated as

$$\lambda(T)^{-1} = \frac{1}{\pi(\mathrm{T} - E_g)\cdot F(T - E_g)} \iint_D \mathrm{Im}\left[\frac{-1}{\varepsilon(\omega, q)}\right]\frac{1}{q}\mathrm{d}q\mathrm{d}\omega\,, \quad (7)$$

$$D = \left\{ (\omega, q) \,\middle|\, E_g \le \omega \le \left(T - E_g - E_v\right), q_- \le q \le q_+ \right\}, \quad (8)$$

$$q_\pm = \sqrt{(T - E_\mathrm{g})\left(2 + (T - E_\mathrm{g})/c^2\right)} \pm \sqrt{(T - E_\mathrm{g} - \omega)\left[2 + (T - E_\mathrm{g} - \omega)/c^2\right]}. \quad (9)$$

As shown in Equation (8), the minimum electron energy loss $\omega_{min}$ is $E_g$, and the maximum energy loss $\omega_{max}$ is the energy difference between incident electron energy and the bottom of conduction band. The effect of band gap on IMFP is dependent on the magnitude of $E_g$. However, for the IMFPs of inorganic compounds, the difference is about ±1.5% or less above 100 eV, and increases to about 6.5% at 54.6 eV[16]. For example, $SiO_2$ ($E_g$ = 9.1eV) has a large bandgap, resulting in a large IMFP of ≥10% at 49.5eV[16]. Therefore, it is not appropriate to ignore $E_g$ effects in IMFP calculations in the electron energy region below 100 eV.

Nine materials (Al, Na, Au, GaAs, $SiO_2$, *c*-BN, *β*-carotene, Kapton, Polyacetylene) were selected from the IMFP data calculated by Shinotsuka *et al.* [15,16,17]. Fig. 1 shows their IMFPs as a function of electron energy between 10 eV and 500 keV. Although there are clear differences in IMFPs between materials, it can be seen that all materials show minimum IMFP values in the energy range of 20 to 100 eV. The energy that yields this minimum value and the energy dependence of its vicinity are largely dependent on the shape of the ELF of the material. Further, all materials exhibit a similar energy dependence between approximately 200 eV and 500 keV. In other words, it can be seen that at 200 eV and higher, the IMFP material dependence does not change even if the electron energy changes.

Shinotsuka *et al.* [15,16,17] conducted fitting for the IMFPs of each material using the following equation by adding the relativistic correction to the modified Bethe equation [14] for inelastic electron scattering in solids.

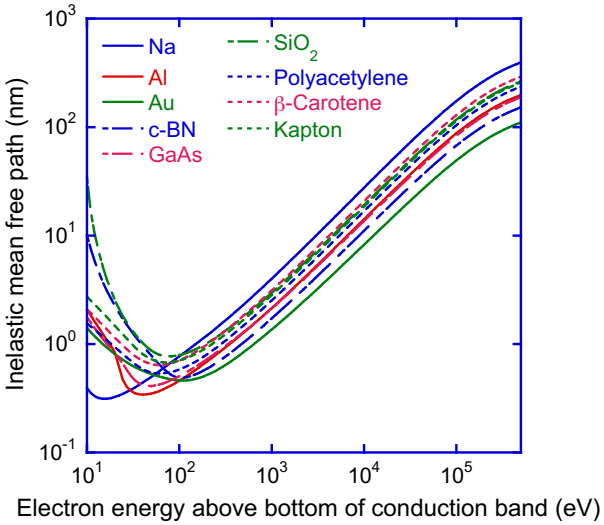


**Fig. 1.** (Color online) Inelastic mean free paths as a function of electron energy for Na, Al, Au, c-BN, GaAs, $SiO_2$, Polyacetylene, *β*-carotene, and Kapton. Solid, long and short dashed, and short dashed lines indicate IMFPs for elemental solids, inorganic compounds, and organic compounds, respectively.

$$\lambda(T) = \frac{\alpha(T)T}{E_p^2\left[\beta(\ln(\gamma\alpha(T)T) - C/T + D/T^2\right]} \quad (10)$$

where $\alpha(T) = \frac{1+T/(2m_ec^2)}{[1+T/(m_ec^2)]^2} \approx \frac{1+T/1021999.8}{(1+T/510998.9)^2}$

The root-mean-square (RMS) deviation between the IMFPs obtained from fitting and each IMFPs calculated individually with FPA was 0.68% for elemental solids [15], 0.60% for inorganic compounds [16], and 0.17% for organic compounds and liquid water [17]. This demonstrates that the energy dependence of the IMFP of each material between 50 eV and 200 keV can be described with the modified Bethe equation.

2) Mermin-GOS algorithm

Abril *et al.* determined the ELF of Equation (4) using the Merin dielectric function $\varepsilon_M(q,\omega)$[23], which is given as [24]

$$\mathrm{Im}\left[\frac{-1}{\varepsilon(q,\omega)}\right] = \mathrm{Im}\left[\frac{-1}{\varepsilon(q,\omega)}\right]_{\mathrm{VB}} + \mathrm{Im}\left[\frac{-1}{\varepsilon(q,\omega)}\right]_{IS} \quad (11)$$

where $\mathrm{Im}[-1/\varepsilon(q,\omega)]_{\mathrm{VB}}$ represents the contribution due to the excitation of the valence electron (outer shell electron), and

it is expressed using $\varepsilon_M(q,\omega)$ as

$$\mathrm{Im}\left[\frac{-1}{\varepsilon(q,\omega)}\right]_{VB} \approx \sum_{i=1}^{L} a_i \, Im\left[\frac{-1}{\varepsilon_M(q,\omega;\omega_i,\gamma_i)}\right], \quad (12)$$

where $L$ represents the number of ELF peaks, and $a_i, \omega_i,$ and $\gamma_i$ represent the strength (oscillator strength), position, and half width of peak $i$, respectively.

Each of these parameters are determined with the following equation, assuming that the optical ELF (ELF at $q = 0$) is approximated as the sum of Drude functions.

$$\mathrm{Im}\left[\frac{-1}{\varepsilon(\omega)}\right] = \sum_{i=1}^{L} A_i \mathrm{Im}\left[\frac{-1}{\varepsilon_M(q=0,\omega;\omega_i,\gamma_i)}\right] \equiv \sum_{i=1}^{L} A_i \frac{\gamma_i \omega \omega_i^2}{\left(\omega^2-\omega_i^2\right)^2+\gamma_i^2\omega^2}. \quad (13)$$

On the other hand, the ELF for the inner shell is given by [25]

$$\mathrm{Im}\left[\frac{-1}{\varepsilon(q,\omega)}\right]_{IS} = \frac{2\pi^2 N}{\omega}\sum_j \alpha_j \sum_{nl} \frac{d f_{nl}^{(j)}(q,\omega)}{d\omega}, \quad (14)$$

where $d f_{nl}^{(j)}(q,\omega)/d\omega$ is the general oscillator strength (GOS) in the hydrogen model for the $j$ number element subshell $(n,l)$. $\alpha_j$ represents the stoichiometry of the $j$ number element in the compound.

Denton *et al.* [26] reported IMFP in the range of 3 eV to 10 keV for Al and Au using the Mermin-GOS algorithm. The integral domain $D$ was set as $\omega_{max} = \min(E/2,\ E - E_F)$, considering the indistinguishability of electrons. In these calculations, the optical ELF is approximated by calculating the contribution of the outer shell electrons in these calculations as seven Drude functions for Au and one Drude function for Al, respectively.

Behar *et al.* calculated IMFP for $HfO_2$ from 10 eV to 10 keV using a similar method[27]. $HfO_2$ IMFPs could be fitted with Equation (10) proposed by Tanuma *et al.*, in energy regions between 40 eV and 10 keV.

de Vera *et al.* [28] calculated IMFP for four organic compounds (PMMA, Kapton, polyacetylene, polyvinyl-2-pyridine) in the energy range from 10 eV to 10 keV by incorporating the Born–Ochkur electron exchange correction[29] into the Mermin-GOS algorithm; the integral domain was the same as that in reference 26. Their calculated IMFP for organic compounds ranging from 10 eV to 10 keV was sufficiently fitted with Equation (10).

Garcia-Molina *et al.* calculated IMFP with Mermin-GOS in the range from 10 eV to 10 keV for liquid water, DNA, protein, lipid, carotene, sugar, and ice [30]. In these calculations, they corrected the electron exchange effect using the Born–Ochkur approximation. Instead of optical ELFs for the target materials, they directly used EELS (electron energy-loss spectroscopy) data, approximated the appropriate number for each compound with the Drude functions, and set the Mermin ELF parameters (in $q = 0$); the error margin for both the f-sum and KK-sum rules was 2% or less. In addition, $\omega_{max}$ used the following equation considering the ELF energy gap.

$$\omega_{max} = \min\left[\frac{T+E_b}{2}, T - E_{\mathrm{Pauli}}\right], \quad (15)$$

where $E_b = E_g$ for the outer shell electrons, and $E_b$ for the inner shell electrons is equal to the ionization energy; it was assumed that $E_{\mathrm{Pauli}} = 4\mathrm{eV}(= E_F)$. They found that the IMFPs of low-energy electrons varied significantly among the series of calculated biomaterials.

de Vera *et al.* [31] divided the ELF involving the outer shell electrons of each material into single excitation and plasmon excitation, and they calculated IMFP in the energy regions from several electron volts to 10 keV by applying the high-order Born approximation for liquid water, Au, Al, and Cu. Meanwhile, it was assumed the Born–Ochkur approximation related to the electron exchange effect could be disregarded in plasmon excitation because it can be differentiated from incident electrons. In order to distinguish the ELFs of the outer shell at $q$ =0 given by Eq. (17) for each excitation, they also introduced a switching function. This allowed us to handle the measured optical ELF by separating them into several single excitations and plasmon excitations. Integral domain $D$ was separated into conductor and non-conductor, and the upper limit of the energy integral for each single excitation was set as $\omega_{max}$. The most significant difference was that the indistinguishability of electrons was limited to single excitation, and plasmon excitation was not applicable. Based on this, the maximum energy loss in plasmon excitation was given by $T$- $E_F$. Two types of excitations were considered for single excitation depending on whether the target material had an energy gap ($E_g$): electron transition to a local discrete energy level and transition to the conduction band; distinct $\omega_{max}$ were given to each. Subsequently, it was reported that the calculated

IMFP values for water, aluminum, gold, and copper correlated well with the obtained experiment data, even in very low energy regions.

3) Super Extended Mermin algorithm (S-EMA)

Da *et al*. [32] enabled the accurate approximation of ELF using unlimited number of Mermin oscillators by permitting negative terms in $a_i$ in Equation (12) to resolve the inconvenience of calculating inner shell electrons and outer shell electrons in Mermin-GOS as individual ELFs. This enabled the approximation of the rapidly changing shape of ELF because of phonon excitation, $E_g$ in low energy regions from the shape at the absorption edge of the inner shell excitation, such as in K, L shells in the ELF in the high-energy regions. Further, they applied this technique to IMFP calculations in several eV to 10 keV for Cu [32], and liquid water [33]. In these calculations, the optical ELF in the range from 0 eV to 10 keV for Cu was approximated with 77 Drude functions. The ELF in the range from $10^{-7}$ eV to 30 keV for liquid water was approximated with 210 Drude functions. The calculated Cu IMFP showed smaller values in low energy regions than the IMFP calculated with FPA and Mermin-GOS. Their Cu IMFPs calculated by S-EMA agrees well with the Cu IMFPs obtained by Tanuma *et al*.[34] from EPES in the energy range from 200 eV to 5 keV. In addition, their Cu IMFPs with S-EMA are in good agreement with the Cu IMFPs determined by Bourke *et al.*[35] with XAFS in the energy range from 60 eV to 120 eV.

4) Mermin–Penn Hybrid Approach (MPA)

Nguyen–Truong introduced damping to the Penn algorithm by replacing the Lindhard dielectric function used in FPA with the Mermin dielectric function [36]. This corresponds to handling plasmon lifetimes as finite; that is, unlike the Mermin-GOS algorithm, it is no longer necessary to conduct separate calculations for the inner shell excitation and outer shell excitation and to approximate the optical ELF with many Drude functions. The measured optical ELF data can be used directly as follows, similar to PFA. Equation (5) is changed to the following equation using the Mermin dielectric function.

$$\mathrm{Im}\left[\frac{-1}{\varepsilon(q,\omega)}\right] = \int_0^\infty d\omega_p \mathrm{G}(\omega_p)\mathrm{Im}\left[\frac{-1}{\varepsilon_M(\mathrm{q},\omega;\omega_\mathrm{p})}\right], \quad (16)$$

where G represents an adjustment parameter to ensure that the above equation correlates with the optical ELF ( $q = 0$). It is given by

$$G(\omega) = \frac{2}{\pi\omega^2\gamma_D}\mathrm{Im}\left[\frac{-1}{\varepsilon(\omega)}\right]\sqrt{2\omega\left(\omega^2+\gamma_D^2\right)\left(\sqrt{\omega^2+\gamma_D^2}-\omega\right)}, \quad (17)$$

where $\gamma_D$ represents the damping coefficient, which is an external input parameter. The IMFPs for Al and Au were calculated between 1 eV and 30 keV with this method, and the resulting IMFPs were compared with the measurement values. When $\gamma_D = 1.5$ eV, the Al IMFPs with MPA agreed well with the experimental values in the energy range of 5 to 9 eV. On the other hand, for Au, when $\gamma_D = 2.0$ eV, the IMFP values from 1 eV to 3 eV calculated by MPA were in good agreement with those obtained from the GW+T *ab initio* calculations[37].

Further, band gap correction was incorporated into MPA using the Levine–Louie dielectric function $\varepsilon_{\mathrm{MLL}}$[38], and the IMFPs of water were calculated to be in the energy range of 1 eV to 10 keV [39] (Figure 2). This improvement made it possible to avoid overestimating ELF because of the presence of a large energy gap in water; the determined IMFP agreed well with the experimental data [39].

5) Comparison of IMFPs

A detailed comparison of IMFP values has been conducted by Shinotsuka *et al.*[15,16,17,33] They compared IMFPs calculated by FPA with IMFPs obtained from other calculation methods and with experimental IMFPs, for elemental solids [15], inorganic compounds [16], liquid water [33], and organic compounds [17]. The calculated IMFP values generally agreed well with the energy range between 300 eV and 10 keV.

For example, Fig. 2 shows the IMFP values for liquid water calculated with the various algorithms described in this chapter. Meanwhile, it also shows as reference, the values calculated by Emfietzoglou *et al.* using the Emfietzoglou-Cucinotta-Nikjoo (ECN) model [40], which yields analytic formulae for the arbitrary energy and momentum transfer in ELF($q$,$\omega$) for the liquid water based on experimental data[i]. As mentioned earlier, even in Fig. 2,

[i] "Emfietzoglou *et al*; corrected" in Figure 2 is IMFPs calculated by correcting the second-order Born

the calculated IMFP values agreed well with each other in the electron energies between 300 eV and 10 keV. In the energy region below 100 eV, the IMFP values differ significantly depending on the presence or absence of

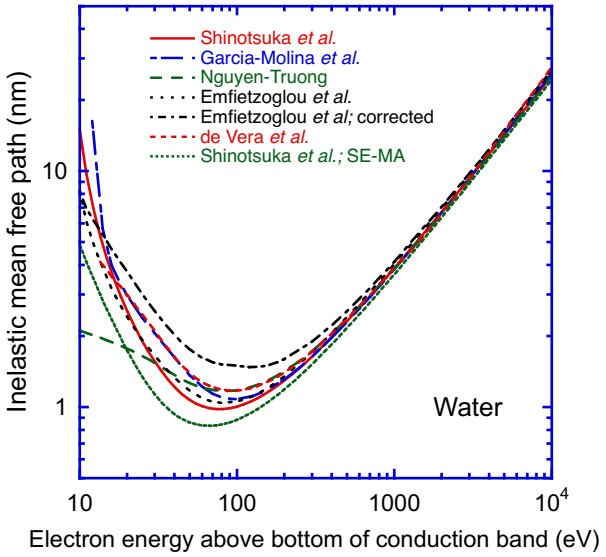


**Fig. 2.** (Color online) Comparison of IMFPs for liquid water calculated from optical ELF ($q$ = 0, ω) with various algorithms. IMFP data were cited from Shinotsuka *et al*. [17] using FPA-BABC, Garcia-Molina *et al*[30] using Mermin GOS, Nguyen-Truong[39] using MPA, Emfietzoglou *et al*.[40] de Vera *et al*.[32] using Mermin-GOS with a high-order Born approximation, and Shinotsuka *et al*. using SE-MA [33]

electron exchange and $E_g$ corrections.

Da *et al.* also conducted detailed comparisons of FPA and Mermin-GOS using model Drude functions as the starting point for calculations instead of the measured values for ELF [41]. They reported that the Mermin-GOS IMFP was approximately 5% smaller than the FPA IMFP at energies from 1 eV to 10 keV. Further, they compared IMFPs obtained from S-EMA, Mermin-GOS, and FPA for Al, Si, Cu, Au, and MgO using measured ELF [42].

## 3. IMFP predictive equation

The TPP-2M equation [14] developed by Tanuma *et al*. using IMFP values in energy ranges from 50 eV to 2 keV in 27 elements and 15 inorganic compounds is widely used for estimating IMFP values. Furthermore, Shinotsuka *et al*. [15] developed a relativistic TPP-2M that extends the upper limit of the application of this equation to a range from 2 keV to 200 keV. The relativistic TPP-2M equation comprises the extended Bethe equation that incorporates the relativistic correction shown in Equation (10) and the conventionally used four parameters shown below. The range of applications is from 50 eV to 200 keV.

$$\beta = -1.0 + \frac{9.44}{\left(E_p^2 + E_g^2\right)^{0.5}} + 0.69\rho^{0.1} \left(\mathrm{eV}^{-1}\ \mathrm{nm}^{-1}\right), \quad (18a)$$

$$\gamma = 0.191\rho^{-0.5} \quad \left(\mathrm{eV}^{-1}\right), \quad (18b)$$

$$C = 19.7 - 9.1U \quad \left(\mathrm{nm}^{-1}\right), \quad (18c)$$

$$D = 534 - 208U \quad \left(\mathrm{eV\ nm}^{-1}\right), \quad (18d)$$

where $U = N_v\rho/M = \left(E_p/\,28.816\right)^2$.

The mean RMS deviation (50 eV–200 keV) for each material based on the IMFP values calculated with FPA and IMFPs obtained from the relativistic TPP-2M equation was 11.9% for a group of 41 elemental solids, 10.7% for a group of 42 inorganic compounds, and 7.2% for a group of 14 organic compounds and liquid water. Unfortunately, several materials such as *c*-BN, and diamond exhibit large RMS deviations.

Figures 3 and 4 show the results of comparing IMFPs determined with the TPP-2M equation and those obtained experimentally, using Fe and MgO as examples. These figures show that the IMFP values in Fe and MgO given by the TPP-2M equation are in good agreement with the IMFP values [43,44,45,46,47,48] between 50 eV and 200 keV measured using various methods.

## 4. Summary

This article described the recent developments in IMFP calculations, which use dielectric response functions ε(q, ω) and optical ELF as the key parameters. A vast amount of effort has been expended to develop and improve the algorithms required to estimate $\mathrm{Im}[-1/\epsilon(q,\omega]$ in $q > 0$ from optical ELF $\mathrm{Im}[-1/\epsilon(\omega]$. IMFPs calculated with various algorithms agreed well with each other at electron energies above 300 eV for most materials. However, in the energy region below 200 eV, there was a large variation. In addition, the energy dependence of IMFPs could be expressed by the extended Bethe equation (10) for electron energies above 50 eV. In the IMFP calculated from FPA, the material dependence could be expressed with the TPP-2M equation. The TPP-2M equation, then, indicate that the

approximation and electron exchange to the ECN model.

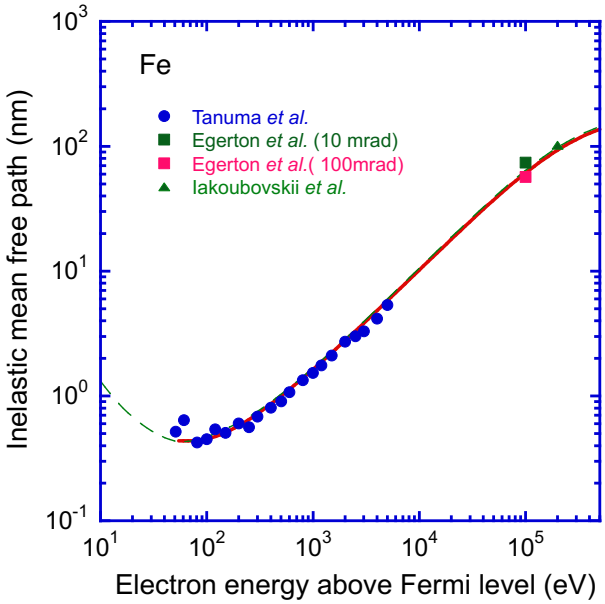


Fig. 3. (Color online) Comparison of calculated IMFPs with measured IMFPs for Fe. The solid line indicates IMFPs calculated with the relativistic TPP-2M equation, and the long-dashed line indicates IMFPs calculated from FPA. The symbols indicate IMFPs measured by Tanuma *et al*. [43], Egerton *et al*. [44], and Iakoubovskii *et al*. [45]

IMFP values between 50 eV and 200 keV can be estimated from simple physical quantities such as the density of the target sample and the number of valence electrons.

The following points are issues that should be addressed. ELF is an important physical quantity that determines the accuracy of IMFP calculations; however, there are many problems with the number and accuracy. However, now that ELFs can be calculated from first-principles calculations, ELFs for many materials should be compared and evaluated with experimental values, and this information should be maintained as a database.

The treatment and evaluation of electron exchange effects, $E_g$ effects, and related integral regions are important remaining issues for IMFP calculation methods based on dielectric response functions. Furthermore, the Born approximation describes the interaction between the incident high-energy electrons and the electrons in the solid. Considering that the energy difference between the outer shell electrons and incident electrons is small in the low energy region below about 100 eV, it may be necessary to reconsider the effect of this higher order correction and the validity of the Born approximation. In such cases, comparison with measured IMFP values would be very important. Although this point is not addressed in this report, it is hoped that accurate measured IMFP values over a wide energy range for many materials will be available in the near future.

**References**

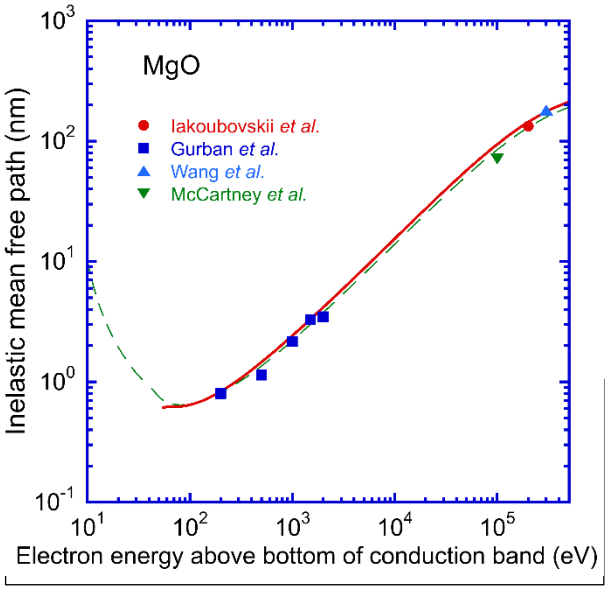


[1] http://kikakurui.com/k0/K0147-1-2017-01.html
[2] C. J. Powell, A. Jablonski, J. Phys. Chem. Ref. Data, **28**, 19 (1999).
[3] U. Fano, Ann. Rev. Nucl. Sci. **13**, 1 (1963).
[4] J. M. Fernandez-Varea, F. Salvat, M. Dingfelder, D. Liljequist, Nucl. Instrum. Meth. Phys. Res. B **229**, 187 (2005).
[5] J.M. Fernandez-Varea, D. Liljequist, S. Csillag, R. Raty, F. Salvat, Nucl. Instrum. *Methods Phys. Res. B* **108** , 35 (1996).
[6] H. Shinotsuka, S. Tanuma S, C. J. Powell, D. R. Penn, Surf Interface Anal. **47**, 871 (2015).; ibid, Surf. Interface Anal., **47**, 1132 (2015).
[7] D. R. Penn : Phys. Rev. B.**35**, 482 (1987).
[8] J. Lindhard, K. Dan. Vidensk. Mat.-Fys. Medd. **28**, 1

(1954).
[9] H. T Nguyen-Truong, J. Phys. Chem. C., 119, 7883 (2015).
[10] S. Tanuma: Vacuum and Surface Science, **65**, 102 (2022).
[11] S. Tanuma, C. J. Powell, D.R. Penn, Surf. Interface Anal. **11**, 577 (1988).
[12] S. Tanuma, C. J. Powell, D.R. Penn, Surf. Interface Anal., **17**, 911 (1991).
[13] S. Tanuma, C. J. Powell, D.R. Penn, Surf. Interface Anal., **17**, 927 (1991).
[14] S. Tanuma, C. J. Powell, D. R. Penn, Surf. Interface Anal., **21**, 165 (1994).
[15] H. Shinotsuka, S. Tanuma, C. J. Powell, D. R. Penn, Surf. Interface Anal., **47**, 871 (2015).
[16] H. Shinotsuka, S. Tanuma, C. J. Powell, D. R. Penn, Surf. Interface Anal., **51**, 427 (2019).
[17] H. Shinotsuka, S. Tanuma, C. J. Powell, D. R. Penn, Surf. Interface Anal., **54**, 534 (2022).
[18] http://www.wien2k.at/; P. Blaha, K. Schwarz, G. K. H. Madsen, D. Kvasnicka, J. Luitz, WIEN2k, An Augmented Plane Wave + Local Orbitals Program for Calculating Crystal Properties (Karlheinz Schwarz, Tech. Universität Wien, Austria), 2001.ISBN 3-9501031-1-2.
[19] http://feffproject.org/; A. L. Ankudinov, C. Bouldin, J. J. Rehr, J. Sims, H. Hung, Phys. Rev. B 65, 104107 (2002).
[20] H. Shinotsuka, H. Yoshikawa, S. Tanuma, e-Journal of Surface Science and Nanotechnology 19, 70 (2021).
[21] http://feffproject.org/; A. L. Ankudinov, C. Bouldin, J. J. Rehr, J. Sims, H. Hung, Phys. Rev. B 65, 104107 (2002).
[22] T. Boutboul T, Akkerman A, Breskin A, Chechik R, J. Appl. Phys., 79, 6714 (1996).
[23] N. D. Mermin, Phys. Rev. B, 1, 2362 (1970).
[24] I. Abril, R. Garcia-Molina, C. D. Denton, J. Perez-Peres, R. Arista, Phys. Rev. A 58, 357 (1998).
[25] S. Heredia-Avalos, R. Garcia-Molina, J. M. Fernández-Varea, I. Abril, Phys Rev. A 72, 052902 (2005).
[26] Cristian D. Denton, Isabel Abril, Rafael Garcia-Molina, Juan C. Moreno-Marín, Santiago Heredia-Avalosc, Surf. Interface Anal. 40, 1481 (2008).
[27] Moni Behar, Raul C. Fadanelli, Isabel Abril, Rafael Garcia-Molina, Cristian D. Denton, Luiz C. C. M. Nagamine, Néstor R. Arista., PHYSICAL REVIEW A 80, 062901 (2009 ).
[28] Pablo de Vera, Isabel Abril, Rafael Garcia-Molina, J. Appl. Phys. **109**, 094901 (2011).
[29] J. M. Ferna´ndez-Varea, R. Mayol, D. Liljequist, and F. Salvat, J. Phys.: Condens. Matter 5, 3593 (1993).
[30] Rafael Garcia-Molina, Isabel Abril, Ioanna Kyriakou, Dimitris Emfietzoglou, Surf. Interface Anal., **49**, 11–17 (2017).
[31] Pablo de Vera, Isabel Abril, Rafael Garcia-Molina, J. Phys. Chem. C, **123**, 2075 (2019).
[32] B. Da, H. Shinotsuka, H. Yoshikawa, Z. J. Ding, S. Tanuma, Phys. Rev. Lett. **113**, 063201 (2014).
[33] H. Shinotsuka, S. Tanuma, C. J. Powell, D. R. Penn, Surf. Interface Anal., **49**, 238 (2017).
[34] S. Tanuma, H. Yoshikawa, N. Okamoto, and K. Goto, J. Surf. Anal. **15,** 195 (2008).
[35] J. D. Bourke and C. T. Chantler, Phys. Rev. Lett. **104**, 206601 (2010).
[36] Hieu T. Nguyen-Truong, J. Phys. Chem. C **119,** 7883 (2015).
[37] V. P. Zhukov, E. V. Chulkov,P. M. Echenique, Phys. Rev. B, **73**, 125105 (2006).
[38] Z. H. Levine, S. G. Louie, Phys. Rev. B, **25**, 6310 (1982).
[39] Hieu T. Nguyen-Truong, J. Phys.: Condens. Matter, **30**, 155101 (2018).
[40] D. Emfietzoglou, G. Papamichael, H. Nikjoo, Radiat Res.,**188**, 355 (2017).
[41] B. Da, H. Shinotsuka, H. Yoshikawa, S. Tanuma, Surf. Anal. **51,** 627 (2019).
[42] B. Da, X. Liu, L. H. Yang, J. M. Gong, Z. J. Ding, H. Shinotsuka, J. W, Liu, H. Yoshikawa, S. Tanuma, J. Appl. Phys. **131**, 175301 (2022)
[43] S. Tanuma, T. Shiratori, T. Kimura, K. Goto, S. Ichimura, C. J. Powell, Surf. Interface Anal. **37**, 833(2005).
[44] R.F. Egerton, Electron Energy-loss Spectroscopy in the Electron Microscope, 3rd edition, Springer, New York, 2011.
[45] K. Iakoubovskii, K. Mitsuishi, Y. Nakayama, K. Furuya, Phys. Rev. B **77**, 104102 (2008).
[46] S. Gurban, G. Gergely, J. Toth, D. Varga, A. Jablonski, M. Menyhard. Surf Interface Anal., **38**, 624 (2006).
[47] Z. L. Wang, A. J. Shapiro, Ultramicroscopy, **60**, 115 (1995).
[48] M. R. McCartney, M. Gajdardziska-Josifovska, Ultramicroscopy, **53**, 283 (1994).